Original Paper

Synthesis of $WO_3 \cdot 0.33H_2O$ Nanoneedles by Hydrothermal Treatment of Ion-Exchanged Precursor

Mohamed ELNOUBY[1], Kazuo KURUMA[1], Eri NAKAMURA[1], Hiroya ABE[1,*]
Yoshikazu SUZUKI[2], Makio NAITO[1]

[1]Joining and Welding Research Institute, Osaka University, 11-1 Mihogaoka, Ibaraki, Osaka 567-0047
[2]Faculty of Pure and Applied Sciences, University of Tsukuba, 1-1-1 Tennodai, Tsukuba 305-8573

Received September 19, 2013; E-mail: h-abe@jwri.osaka-u.ac.jp

A facile route for synthesis of $WO_3 \cdot 0.33H_2O$ nanoneedles via hydrothermal treatment of an aqueous ion-exchanged precursor has been demonstrated. The effects of hydrothermal conditions such as reaction temperature and time on the morphology and structure of $WO_3 \cdot nH_2O$ have been studied systematically. The $WO_3 \cdot 0.33H_2O$ with an orthorhombic structure and needle-like morphology was synthesized at 120 °C for 5 h. No significant change in the structure and morphology was observed with increasing reaction time to 24 h. At the temperature, the $WO_3 \cdot 0.33H_2O$ grew preferentially along the [100] direction, and was eventually enclosed by {001}, {010} and {110} facets. The observed needle-like evolution has been explained based on the crystal structure of orthorhombic $WO_3 \cdot 0.33H_2O$. The $WO_3 \cdot 0.33H_2O$ nanoneedle was fully dehydrated when it was heated at 350 °C in air. Phase transformation to the hexagonal WO_3 was induced by this dehydration.

Key Words: *Tungsten Hydrous Oxide*, *Nanostructure*, *Acid Precipitation Method*, *Ion-Exchanged Precursor*

1. Introduction

Tungsten trioxide and its hydrates ($WO_3 \cdot nH_2O$) have been extensively studied because of their crystal polymorphism[1], intriguing physical and chemical properties[2-4] and widespread applications[5-8]. Among them, $WO_3 \cdot 0.33H_2O$ has been of interest owing to its unique structure[9,10], that is, layers built up by corner shared WO_6 octahedral forming six-membered rings, with water molecules between these planes. Recently, synthetic strategy for nanostructures of $WO_3 \cdot 0.33H_2O$ and their dehydrated hexagonal WO_3 has been a focused subject due to the concerns in both fundamental science and technological applications[11-16]. In particular, one-dimensional nanostructures such as nanoneedles and nanofibers have been attracted much attention because they not only can provide unique properties[13,16] but also can be used as building blocks for functional micro/nanostructured materials[14-16].

Hydrothermal treatment of acidified precursor has been widely investigated to synthesize $WO_3 \cdot 0.33H_2O$ nanoneedles[13,17-19]. This precursor is usually prepared by acidification of Na_2WO_4 solution with HCl, which contains impurity ions of Na^+ and Cl^-. Gerand et al. synthesized $WO_3 \cdot 0.33H_2O$ nanoneedles using the acidified precursor when heating at 120 °C[18]. In addition, it has been reported that NaCl[13,19] or the sulfate salt[20] act as effective capping agents for formation of one-dimensional evolution of $WO_3 \cdot 0.33H_2O$. However, under the utilization of the acidified precursor and the inorganic salts, the unavoidably contaminated cations such as Na^+ in the final products may result in negative effects on the performances of materials[21].

Ion-exchanged precursor is an alternative acidified precursor[2,22], which is prepared by acidification only through a protonated cation-exchange resin. It contains negligible small amount of the impurity ions. Recently, we have utilized this precursor for synthesis of $WO_3 \cdot nH_2O$, and observed a dominant two-dimensional growth of $WO_3 \cdot H_2O$ under a relatively low temperature (50 °C), resulting in nanoplatelet morphology[23]. Mo et al. obtained nanorods of $WO_3 \cdot 0.33H_2O$ and h-WO_3 mixed phases at 180 °C for 24 h[24]. However, since there are only a few works available in the published literature on the hydrothermal treatment of ion-exchanged precursor, it has been still remained unclear if the impurity-free route can be utilized for the one-dimensional growth of $WO_3 \cdot 0.33H_2O$.

In this study, a facile route for synthesis of pure $WO_3 \cdot 0.33H_2O$ nanoneedles via hydrothermal treatment of an aqueous ion-exchanged precursor has been demonstrated. We have systematically examined the effects of hydrothermal conditions on the morphological and structural evolution of $WO_3 \cdot nH_2O$, and proven that the product of pure $WO_3 \cdot 0.33H_2O$ can be obtained by heating at 120 °C for 5 h or the longer reaction time. Morphological and structural examinations revealed that the $WO_3 \cdot 0.33H_2O$ grows preferentially along the [100] direction, resulting in nanoneedle structure. We expect that the synthetic strategy for the one-dimensional nanostructure of $WO_3 \cdot 0.33H_2O$ will receive some benefits as contamination-free route and versatile techniques.

2. Experimental

2.1 Materials

Sodium tungstate dihydrate ($Na_2WO_4 \cdot 2H_2O$, > 99%) was purchased from Kanto Chemical Co. (Japan) and was used without further purification. Strong acid type of Diaion PK228LH cation exchange resin (ion-exchange capacity > 2.05 meq·mL^{-1}) was supplied from Mitsubishi Chemical Co. (Japan). Deionized water (18.2 MΩ·cm) from Sartorius-arium® 61316 system (Germany) was used throughout the experiments.

A glass column with height of 150 mm and 24.6 mm in diameter was used for the ion-exchange process. The glass column was packed with 30 mL of the ion-exchange resin, and then 10 mL of water was passed through the column to wash the resin. This washing step was repeated five times before experiment.

2.2 Sample preparation

0.5 M Na_2WO_4 solution was prepared by dissolving $Na_2WO_4 \cdot 2H_2O$ powder into deionized water. Then, a 10 mL of the solution was loaded on the glass column, and let it flow down through the resin bed with a rate of 5mL·min^{-1}. The acidified precursor was recovered from the column by elution with deionized water. The precursor was yellowish and transparent. This ion-

exchange treatment was performed in the temperature-controlled chamber at 15 °C. The concentration of W in as-received precursor was estimated to be 0.23−0.24 M by X-ray fluorescence spectroscopy (EDX-800, Shimadzu, Japan).

This ion-exchanged precursor was hydrothermally treated under different reaction temperature (50, 80, 120 and 180 °C) and time (5, 15, 24 h). No additive was employed. After the hydrothermal treatment, the $WO_3 \cdot nH_2O$ powders were obtained, and they were collected by centrifugation and dried in room temperature under vacuum.

2.3 Characterizations

The crystallographic phase of the samples was determined by powder X-ray diffraction (Ultima IV, Rigaku, Japan, Cu-*K*α radiation). Their morphology was examined by scanning electron microscopy (SU-70, Hitachi, Japan) and by transmission electron microscopy (JEM-2100F, JEOL, Japan). The weight loss of the sample was measured by a thermogravimetric analysis (TG/DTA 6200, SII, Japan).

3. Results and discussion

The hydrothermal temperature was varied from 50 to 180 °C, while keeping reaction time for 24 h. The XRD patterns of the samples synthesized at different temperatures are shown in Fig.1. When the reaction was conducted at 50 °C, all peaks were indexed to the orthorhombic $WO_3 \cdot H_2O$ phase (ICDD No.00-043-0679). With temperature increasing to 80 °C, besides the main peaks due to the $WO_3 \cdot H_2O$, secondary peaks originating from the orthorhombic $WO_3 \cdot 0.33H_2O$ phase (ICDD No.01-072-0199) appeared. Further enhancing the reaction temperature to 120 °C, the crystal phase of the sample was identified as pure $WO_3 \cdot 0.33H_2O$. When heating at 180 °C, some characteristic peaks of h-WO_3 were observed, indicating that the orthorhombic $WO_3 \cdot 0.33H_2O$ structure began to transfer to the h-WO_3 phase.

To further investigate the growth of the $WO_3 \cdot 0.33H_2O$, the hydrothermal reaction was also conducted at 120 °C for different reaction time. Figure 2 shows the XRD patterns of the $WO_3 \cdot 0.33H_2O$ obtained for 5, 15 and 24 h. No significant difference is observed for the XRD patterns, indicating that the $WO_3 \cdot 0.33H_2O$ structure was well formed even for relatively short reaction time of 5 h.

The morphologies of the samples obtained at 120 °C for 5 and 24 h are shown in Fig.3, respectively. On the basis of the SEM observation, these samples were composed of a large quantity of nanoneedles. The width and length of the nanoneedles did not significantly depend on the reaction time, indicating also that the needle-like morphology was well developed even for relatively short reaction time of 5 h. Average width of the randomly selected 150 nanoneedles in the sample obtained for 24 h was ~20 nm and the length was up to ~300 nm, reaching an aspect ratio more than 10. The sample obtained at 180 °C for 24 h was also composed of a large quantity of nanoneedles (not shown here). However, the aspect ratio decreased to be ~6, since their width and length were ~40 nm and ~250 nm, respectively. It is suggested that the reaction temperature plays an important role in anisotropic growth of $WO_3 \cdot 0.33H_2O$ nanocrystal.

To understand the detailed structural and morphological characteristics of the $WO_3 \cdot 0.33H_2O$ nanoneedle, the TEM technique was employed. Figure 4(a) shows a typical well-developed nanoneedle found in the sample obtained at 120 °C for 24 h. As can be seen, it consisted of a few or several nanoneedles which elongated and ended triangularly-tapered shape. Figure 4(b)

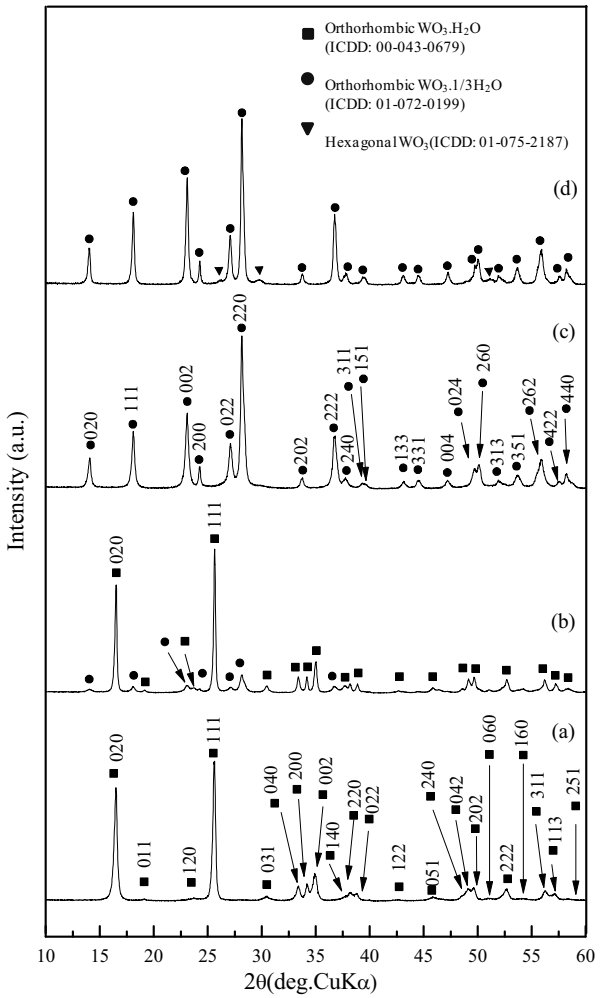

Fig.1 XRD patterns of tungsten oxide hydrates synthesized for 24 h at different reaction temperature of (a) 50, (b) 80, (c) 120 and (d) 180 °C.

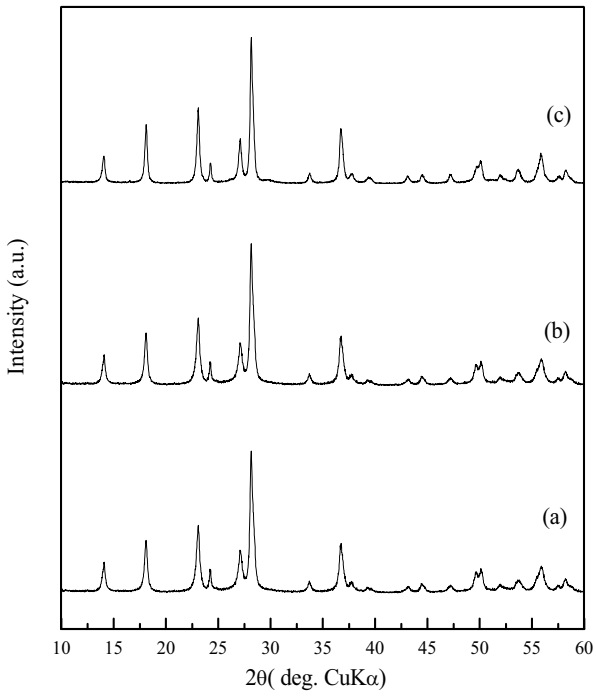

Fig.2 XRD patterns of the nanoneedles synthesized at 120 °C for different reaction time of (a) 5, (b) 15 and (c) 24 h. All peaks can be indexed to orthorhombic $WO_3 \cdot 0.33\ H_2O$ (ICDD No. 01-072-0199).

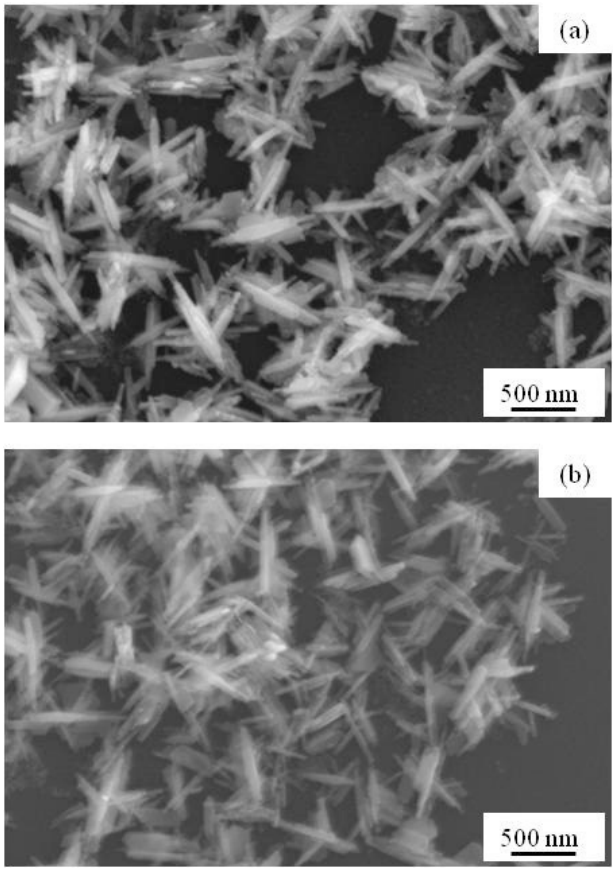

Fig.3 SEM images of $WO_3 \cdot 0.33H_2O$ nanoneedles synthesized at 120 °C for (a) 5 and (b) 24 h.

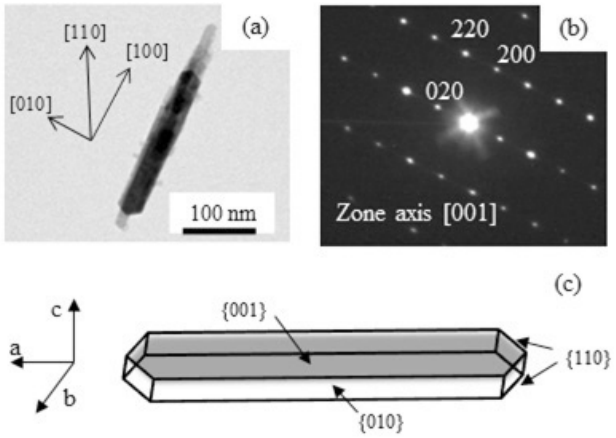

Fig.4 (a,b) TEM image of $WO_3 \cdot 0.33H_2O$ nanoneedle synthesized at 120 °C for 24 h and its corresponding SAED pattern. (c) Crystal model of an elongated $WO_3 \cdot 0.33H_2O$.

shows its corresponding selected area electron diffraction (SAED) pattern. Interestingly, the SAED pattern can be assigned to a phase of single crystalline of the orthorhombic $WO_3 \cdot 0.33H_2O$ located along the [001] zone axis, implying that the nanoneedles had a single crystal nature and their crystallographic orientation remain the same. It provides that top and bottom surfaces of the nanoneedle were of well-defined {001} facet, and the nanoneedle elongated obviously along the [100] direction. Also, the [010] direction is almost perpendicular to adjacent side edge of the nanoneedle, suggesting that the side facets of the nanoneedle were enclosed by the {010} planes. In addition, the [110] direction is almost perpendicular to the tapered side at the tip of the nanoneedle, suggesting that the ends of nanoneedle are enclosed by {110}. From these observations, it can be concluded that the $WO_3 \cdot 0.33H_2O$ crystal grew preferentially along the [100] direction by hydrothermal treatment at 120 °C and was eventually enclosed by {001}, {010} and {110} facets as illustrated in Fig.4(c). The nanoneedles synthesized in the present condition were mainly aligned and stacked structure as shown in Fig.4. We also observed other oriented aggregation structures, and this topic will be reported in a near future.

Figure 5 shows the weight loss behavior of the $WO_3 \cdot 0.33H_2O$ nanoneedles for temperatures from 25 °C to 500 °C in air measured by TGA. It is clear that the sample had an obvious weight loss around 250 °C and was almost completely dehydrated at around 350 °C. The amount of the structural water of the sample was calculated from the weight loss difference between 150 °C and 500 °C. As a result, it corresponded to about $0.4H_2O$ per mole of WO_3. The amount of the structural water estimated was a little higher than theoretical value of 0.33. In this time, we have not taken carefully account of amount of physically adsorbed water trapped between nanoneedles. If it is removed sufficiently, the value would be close to the theoretical one. Based on the TGA curve, the sample was annealed at 350 °C in air to remove the structural water and it was confirmed that the crystalline phase was transformed to the h-WO_3 by the dehydration as shown in Fig.6.

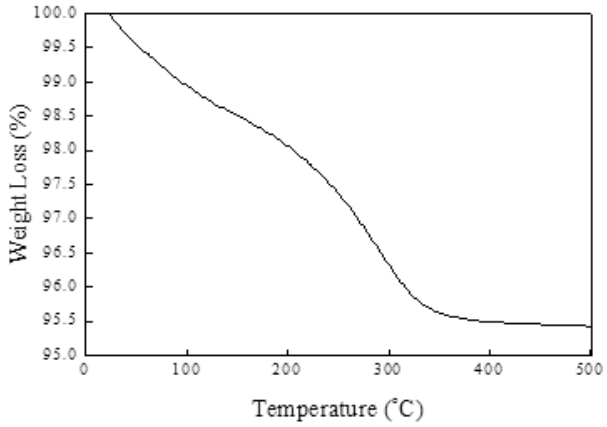

Fig.5 TGA curve of $WO_3 \cdot 0.33H_2O$ sample synthesized at 120 °C for 24 h.

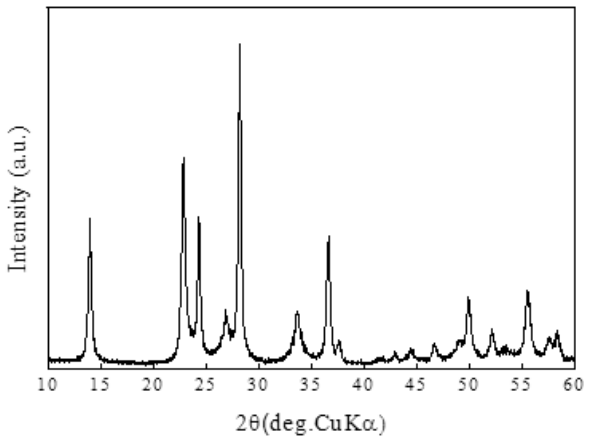

Fig.6 XRD pattern of WO_3 sample obtained after annealing at 350 °C for 1 h in air. All peaks can be indexed to hexagonal WO_3 (ICDD No. 01-075-2187).

As demonstrated in this study, the reaction temperature plays an important role in controlling the morphology and structure of $WO_3 \cdot nH_2O$. The nanoneedles of pure $WO_3 \cdot 0.33H_2O$ phase were first time obtained from the ion-exchanged precursor at 120 °C. The results were reproducible and indicate that phase formation of $WO_3 \cdot 0.33H_2O$ and its one-dimensional growth well promotes even without any inorganic additives such as NaCl and Na_2SO_4. Peroxo-polytungstic acid solution has been also known as impurity-free aqueous precursor[25]. However, hydrothermal treatment of the peroxo-polytungstic acid solution did not produce nanoneedle, but nanodisc $WO_3 \cdot 0.33H_2O$[11].

It has been known that all $WO_3 \cdot nH_2O$ are formed of layers built up by corner sharing [WO_6] octahedral, with water molecules between these planes. Formation of $WO_3 \cdot nH_2O$ in acidified precursor is generally explained as follows[22,26]. The intermediate [$WO(OH)_4(OH)_2$] is formed in the acidified precursor at the initial period of aging, where one water molecule is bonded along to the *z*-axis opposite to the W=O bond while the four OH groups are in the equatorial *x*-*y* plane. Then, oxolation reaction along to the equivalent *x*- and *y*- directions leads to layered structure. As we reported recently, the reaction promotes to form corner-sharing their four equatorial oxygen atoms of octahedra by aging at 50 °C, resulting in $WO_3 \cdot H_2O$ phase[23]. On the other hand, it was found in this study that more open structure with forming six membered rings can be formed when heating up to 120 °C, resulting in $WO_3 \cdot 0.33H_2O$ phase. Since the ion-changed precursor does not contain any structure-directing species, the dielectric constant of water would play an important role. As Livage and Guzman discussed[22], the dielectric constant of water decreases as the temperature increases, and then electrostatic repulsions between highly charged W^{6+} ions become stronger, which lead to the formation of the more open structures such as hexagonal $WO_3 \cdot 0.33H_2O$. However, the detailed mechanism of formation of the $WO_3 \cdot 0.33H_2O$ phase needs to be further explored.

The observed preferential growth of $WO_3 \cdot 0.33H_2O$ along [100] direction can be explained from the crystal growth habit of $WO_3 \cdot 0.33H_2O$. As well known, crystal growth along the direction perpendicular to the face with the highest surface free energy possesses the fastest growth rate, leading to exposure of the lower-energy faces. In the orthorhombic $WO_3 \cdot 0.33H_2O$ structure, the surface free energy of different faces have the order of {100} > {110} > {010} > {001}[11]. On this basis, the fastest crystal growth occurs in the [100] direction and the {001}, {010} and {110} facets are expected as the exposed surfaces in $WO_3 \cdot 0.33H_2O$. This expectation agrees with our experimental results.

4. Conclusions

We have successfully synthesized $WO_3 \cdot 0.33H_2O$ nanoneedles by the additive-free hydrothermal treatment. It was found that the reaction temperature plays an important role on the one-dimensional growth of $WO_3 \cdot 0.33H_2O$, and the nanoneedles were produced at 120 °C even for relatively short reaction time of 5 h. The morphological evolution of the nanoneedle has been explained based on the crystal structure of $WO_3 \cdot 0.33H_2O$. The present synthesis route provides a facile and impurity-free approach for synthesis of $WO_3 \cdot 0.33H_2O$ nanoneedles. It is expected that the nanoneedles can be applied to wide areas and building blocks for constructing functional nanostructures.

Acknowledgments

This work was partly supported by Grand-in-Aid for Exploratory Research (24656442) from the Ministry of Education, Culture, Sports, Science and Technology of Japan, and by the Cooperative Research Program of Institute for Joining and Welding Research Institute, Osaka University.

References

1) C. Guery, C. Choquet, F. Dujeancourt, J. M Trascon, J. C. Lassegus, *J. Solid State Electrochem.*, **1997**, *1*, 199.
2) C. Santaro, M. Odziemkowski, M. Ulmann, J. Augustynski, *J. Am. Chem. Soc.*, **2001**, *123*, 10639.
3) Y. P. Xie, G. Liu, L. Yin, H-M. Cheng, *J. Mater. Chem.*, **2012**, *22*, 6746.
4) S-H. Baeck, K-S. Choi, T. F. Jaramillo, G. D. Stucky, *Adv. Mater*., **2003**, *15*, 1269.
5) C. Cosa, C. Pinheiro, I. Henriques, C. A. Laia, *ACS Appl. Mater. Interfaces*, **2012**, *4*, 1330.
6) D. Li, G. Wu, G. Gao, J. Shen, F. Hung, *ACS Appl. Mater. Interfaces*, **2011**, *3*, 4573.
7) R. Archrya, X. A. Cao, *Appl. Phys. Lett.*, **2012**, *101*, 053306.
8) W. Mickelson, A. Sussman, A. Zettl, *Appl. Phys. Lett.*, **2012**, *100*, 173110.
9) M. Figlarz, *Prog. Solid State Chem.*, **1989**, *19*, 1.
10) B. Gerand, D. Nowogrocki, J. Guenot, M. Flglarz, *J. Solid State Chem.*, **1979**, *29*, 429.
11) L. Zou, M. Yu, P. Lu, J. Wei, Y. Qian, Y. Wang, C. Yu, *Cryst. Growth Des.*, **2008**, *8*, 3993.
12) J. Li, J. Huang, C. Yu, J. Wu, L. Cao, K. Yanagisawa, *Chem. Lett.*, **2011**, *40*, 579.
13) X. C. Song, Y. F. Zheng, H. Y. Yin, *Curr. Nanosci.*, **2011**, *7*, 120.
14) J. Li, J. Hung, J. Wu, L. Cao, Q. Li, K. Yanagisawa, *CrystEngComm*, **2013**, *15*, 7904.
15) Z. Jiao, J. Wang, L. Ke, X. W. Sun, H. V. Demir, *ACS Appl. Mater. Interfaces*, **2011**, *3*, 229.
16) J. Yang, L. Jiao, Q. Zhao, Q. Wang, H. Gao, Q. Huan, W. Zheng, Y. Wang, H. Yuan, *J. Mater. Chem.*, **2012**, *22*, 3699.
17) J. Pfeifer, C. Guifang, P. T-Buxbaum, B. A. Kiss, M. F-Jahnke, K. Vadasdi, *J. Solid State Chem.*, **1995**, *119*, 90.
18) B. Gerand, G. Nowogrocki, M. Figlarz, *J. Solid Sate Chem.*, **1981**, *38*, 312.
19) J. Wang, E. Khoo, P. S. Lee, J. Ma, *J. Phys. Chem. C*, **2009**, *113*, 9655.
20) Z. Gu, H. Li, T. Zhai, W. Yang, Y. Xia, Y. Ma, J. Yao, *J. Solid State Chem.*, **2007**, *180*, 98.
21) H. Zhang, G. Duan, Y. Li, X. Xu, Z. Dai, W. Cai, *Cryst. Growth Des.*, **2012**, *12*, 2646.
22) J. Livage, G. Guzman, *Solid State Ion.*, **1996**, *84*, 205.
23) M. Elnouby, K. Kuruma, E. Nakamura, H. Abe, M. Naito, Y. Suzuki, *J. Ceram. Soc. Jpn.*, in press.
24) R-F. Mo, G-Q. Jin, X-Y. Guo, *Mater. Lett.*, **2007**, *61*, 3787.
25) J. Oi, A. Kishimot, T. Kudo, *J. Solid State Chem.*, **1992**, *96*, 19.
26) J. Yang, W. Li, J. Li, D. Sum, Q. Chen, *J. Mater. Chem.*, **2012**, *22*, 17744.